Research Square

Preprints are preliminary reports that have not undergone peer review.
They should not be considered conclusive, used to inform clinical practice,
or referenced by the media as validated information.

Intraseasonal Variability of the Kuroshio at 18°N Observed by Mooring Array in 2018-2020

Xin Yuan
Institute of Oceanology, Chinese Academy of Sciences
Qingye Wang (wangqy@qdio.ac.cn)
Institute of Oceanology, Chinese Academy of Sciences
Jie Ma
Institute of Oceanology, Chinese Academy of Sciences
Shijian Hu
Institute of Oceanology, Chinese Academy of Sciences
Dunxin Hu
Institute of Oceanology, Chinese Academy of Sciences

Research Article

Keywords: kuroshio, transport, velocity, intraseasonal, variability

Posted Date: June 7th, 2021

DOI: https://doi.org/10.21203/rs.3.rs-583030/v1

License: This work is licensed under a Creative Commons Attribution 4.0 International License.
Read Full License

Abstract

Based on direct measurements of the Kuroshio current velocity at 18°N by an array of three moorings from January 2018 to February 2020, the intraseasonal variability (ISV) of the Kuroshio and possible dynamic mechanism are studied. The Kuroshio transport in the upper 350m between 122.7°E and 123.3°E is estimated to be 6.5 Sv ± 2.6 Sv. It is revealed for the first time that both the current velocity and volume transport the Kuroshio at 18°N have a significant 50-60-day ISV, which contributes to over 30% of the total variance. Further analysis indicates the ISV of the Kuroshio is caused by the westward propagating eddies with a wavelength of about 633 km and a propagation speed of about 13 cm/s. In addition, the transport mode (74.2%) of the Kuroshio at 18°N is dominant, rather than the migration mode (11.6%). That is different from the Kuroshio east of Taiwan. The findings of this study will highlight the important role of westward Rossby waves (eddies) with a finite wavelength in modulating the intraseasonal variability of the Kuroshio transport near its origin.

Introduction

The Kuroshio is a poleward western boundary current in the North Pacific, originating from the east of the Luzon and flowing along the eastern coast of Taiwan and the continental slope of the East China Sea, and finally reaching to the southeast coast of Japan[1]. It is essentially the northward branch of the North Equatorial Current (NEC), transporting large amounts of water mass, heat, and salt from tropical to extratropical regions. Not limited to the ocean itself, but also the exchange of matter and energy between the sea and the air along its path[2]. Therefore, a comprehensive understanding of its variability is required.

Until now, the areas where we have paid more attention to the Kuroshio research are the east of the Luzon Strait[3–6], east of Taiwan[7–11], southeast of the East China Sea continental slope[12–15], and the south of Japan[16–18]. However, few papers are focusing on the variability of the Kuroshio near its origin in previous studies.

In the past two decades, the research on the variability of the Kuroshio near its origin is mainly carried out with the support of two major research projects. One of them is a series of studies under the Origins of the Kuroshio and Mindanao Current (OKMC) program funded by the U.S. Office of Naval Research[19]. Such as, based on observational data collected from two ship surveys in May 2011 and May 2012, Gordon et al.[20] revealed the initiation of the Kuroshio near 16.5°N and estimated the Kuroshio transport is 9.2 Sv (Sverdrup, 1Sv = 10^6 m^3/s) and 14.3 Sv across the 16°30’N section (range:122.4°E to 124.3°E, upper 600m), corresponding to the 10 Sv and 16.7 Sv across the 18°20’N section. At the same time, a longer-term observation with an array of six acoustic Doppler current profiler (ADCP) moorings was along 18.75°N (before the Kuroshio enters the Luzon Strait) between 122°E and 122.87°E during June 2012 to June 2013[21]. The observed results show the Kuroshio transport has an annual mean about 15 Sv computed and suggested that the seasonal variation of it modulated by the seasonal variation of the

impinging mesoscale eddies. For more schematic descriptions of the above mooring position, the readers can refer the Fig. 3[19].

Besides the OKMC program, there is also a field experiment focusing on the variability of the Kuroshio east of Luzon Island supported by the Northwestern Pacific Ocean Circulation and Climate Experiment program. Analyzing the mooring data deployed at 18°N that spanned 8 months from November 2010 to July 2011, a significant intraseasonal variability (ISV) of about 70–80 days of the Luzon Undercurrent (LUC) is exposed[22]. Based on model simulation from Hybrid Coordinate Ocean Model (HYCOM), Wang et al.[23] further suggested that the ISV of the subsurface LUC are vertically coherent with surface Kuroshio Current, indicating that the ISV of the LUC is dominated by eddies with diameters of about 200–300 km and extending from sea surface to an intermediate layer east of the Luzon Island. Combined with the subsequent second set of mooring recovered in October 2012, Chen et al.[24] describe the low-frequency variability of the Kuroshio during the two years observational period.

Compare to the observation data analyzed in Gordon et al.[20] and Chen et al.[24], the latter has a longer period in site mooring observations that last over one year. However, there is only one set of mooring was equipped to measure, instead of a mooring array. Fortunately, this regret has been improved in the study. The precious observation data utilized in the research is one of the highlights of this article. This observation data has a longer time span than Gordon et al.[20], more than two years (766 days); a wider spatial area than Chen et al.[24], an array of three moorings at ~ 18°N; and a closer to the origin (~ 18°N) of the Kuroshio than Lien et al.[21]. Until the publication of this article, there are gaps in the research on the ISV of the Kuroshio near its origin using direct mooring observation data. Therefore, the primary objective of this study is to describe the ISV characteristics of the Kuroshio near its origin (at 18°N) and discuss it, including the velocity variability at each mooring site and transport variability through the 18°N section. Generally speaking, there is an abundant mesoscale eddy region east of the Luzon island/Strait, which is generated through the baroclinic instability of the surface eastward flowing North Pacific Subtropical Countercurrent (STCC) and the subsurface westward flowing NEC system[25–29]. Meantime, previous studies report that westward propagating eddy-Kuroshio interaction processes revealed by mooring observations[21,30–32]. Thence, the secondary aim of this study is to explore what caused the observed ISV of the Kuroshio and whether it is related to the mesoscale eddies from the Pacific.

Results

Mean structure

East of Luzon Island (~18°N), the Kuroshio basically flows along the north-south direction (Fig.1a). Therefore, we focus on the meridional velocity of ADCP observed. The observed meridional velocities from three moorings reveal the intensity of the Kuroshio: M1>M2>M3 (Fig. 1b, 1c, and 1d), which indicates that M1 is closer to the axis of the Kuroshio.

In Fig. 2a, the structure of the time-mean meridional velocities shows the maximum of M1, M2, and M3 are 71.9 cm/s (depth: 60 m), 41.8 cm/s (60 m), and 19.9 cm/s (110 m), respectively. This structure indicated that only the eastern part of the Kuroshio current axis was monitored by the array of three moorings, and the Kuroshio near the shore was missing, which is clarified by the HYCOM simulated meridional velocity structure along the 18°N section during the mooring measurements period (Fig. 2b). The simulated result is remarkable consistent with the mooring observations, despite it is a little smaller than the observed value.

ISV of the meridional velocity

At first, we compare the mean velocity with the standard deviation of it at the layer of 60 m, 100 m, and 200 m. The mean velocity (the standard deviation) of M1, M2 and M3 are 72 cm/s (23 cm/s), 41 cm/s (17 cm/s), and 18 cm/s (14 cm/s) at 60 m, respectively. The value is 65 cm/s (20 cm/s), 39 cm/s (15 cm/s), 20 cm/s (12 cm/s) at 100 m and 32 cm/s (14 cm/s), 25 cm/s (11 cm/s), 15 cm/s (8 cm/s) at 200 m. The three moorings all show that the standard deviation of velocity accounts for ~ 1/3 to 2/3 of the mean velocity. Noticeable, the standard deviation is nearly equal to the mean velocity, or even larger at 300–350 m. This suggests that the variability of the meridional velocity is very strong and deserves our research. Besides, the observed meridional velocity also shows obvious ISV of about two months in Fig. 1b, 1c and 1d.

In order to remove the interference of low-frequency signals, we extract the ISV of the velocity by using a 20–120 days Lanczos bandpass filter (Fig. S1). The result shows that the intraseasonal velocity changes of the Kuroshio are consistent in the vertical direction at each mooring site, and the intraseasonal velocity is stronger on the surface layer than the lower layer. Power spectrum density (PSD) analysis for observed intraseasonal velocity shows that the intraseasonal period is 40–60 days at M1, 50–60 days at M2 and M3, and vertical consistency (Fig. 3). Notably, the period with a peak of ~100 days is also significant, but the strongest signal of 50–60 days is mainly considered in this study.

Herein, further analysis of the characteristics of the ISV of the meridional velocity in the latitudinal direction. Considering that the ISV of the Kuroshio has vertical consistency, and the intraseasonal signal is more obvious in the surface (Fig. S1), so we choose an average meridional velocity range of 60–100 m to represent the main variability in the intensity of the Kuroshio. The time series of the Kuroshio intensity in three moorings are shown in Fig. S2a, with average values of 68.0 cm/s, 40.1 cm/s, and 19.1 cm/s, respectively. Similarly, Fig. S2b shows the time series of the intraseasonal velocity of average range 60–100 m. Firstly, the latter suggests that there are synchronized ISV at M1, M2, and M3, and there is almost no lag time. Secondly, though the background flow field at M1, M2, and M3 are largely different, the intensity of the ISV is nearly the same (the standard deviations are 12.1 cm/s, 9.7 cm/s, and 10.0 cm/s, respectively), which implies that they are modulated by the same mechanism. In other words, the ISV of the Kuroshio is consistent in the latitudinal direction.

ISV of the transport

The above analysis of the observed velocity shows that the ISV is consistent in the temporal and spatial structure at three mooring sites. Next, we will analyze the volume transport of the whole section to explore the characteristics of its ISV. According to observed velocity between 0–350 m depth, the annual average of the Kuroshio transport is calculated to be 6.5 Sv and the standard deviation of 2.6 Sv (Fig. 4). It should be noted that the mooring ADCP miss the Kuroshio above 50 m, thereby we used the constant velocity measured at a depth of 60 m to fill. There are two pieces of evidence to support the above approach. (1). According to the consistent results between the observed velocity of 60m depth by moored ADCPs and the surface velocity from the altimeter, which the correlation coefficient is around 0.8; (2). The HYCOM data during the mooring observed period simulate that the meridional velocity is almost consistent in the vertical direction within 0–50 m, and there is little shear as shown in Fig. 2b.

This result is only responsible for the mooring observation region (123.7°E–123.3°E, 0–350 m), however, the Kuroshio can also be seen near the coast (122.2°E–122.7°E) as shown in Fig. 2b. Previous observations suggested that the Kuroshio has a width of about 100–150 km[8,21,33]. In this study, the measured width of the mooring array is 64 km, and there are 54 km away from the coast. If the whole transport along 18°N is twice of the observed, the whole transport of the Kuroshio could be roughly estimated to be about twice as large as our observations (13 Sv). By the way, we also use the HYCOM simulated data of the same period to calculate the result to be 11 Sv between the surface and 350m depth (range 122.2°E–122.7°E). These results are almost consistent with the transport (10 Sv and 16.7 Sv) along 18.3°N section[20] and close to that 15 Sv along the 18.75°N section[21].

In the following, only the actual results observed are discussed. The PSD shows that the observed Kuroshio transport has ISV signal of 50–60 days and 100 days (Fig. 4b), which is consistent with the velocity period of the mooring ADCPs measurements (Fig. 3). Regarding the relationship between intraseasonal transport and intraseasonal velocity at M1, M2, and M3 (Fig. S2b), the coefficient of the two is quite high, with an average value above 0.8 (0.84, 0.87, and 0.72, respectively), which is above the 95% confidence level. The results show that the variability of each mooring is synchronized and consistent with the variability of the whole section.

Moreover, the altimeter data (meridional velocity) during the mooring observation period and over a long period of time (1993–2020) are used to calculate the surface Kuroshio transport ranging from 122.625°E to 123.375°E along the 18.125°N section. The result suggested that the surface Kuroshio also has an ISV period of 50–60 days both the meridional velocity and the transport (not shown), which agrees well with the dominant period of the mooring observed. Thus, the Kuroshio at the observation region has a reliable ISV signal, which is 50–60 days.

The transport mode and migration mode of the observed Kuroshio

The empirical orthogonal function (EOF) analysis has been used to investigate the variance associated with the lateral migration of the Kuroshio core from mooring arrays[8, 34]. Similar to their analysis, we adopt the EOF analysis to decompose the Kuroshio meridional velocity observed into the variation in

transport mode (Fig. 5) and migration mode (Fig. 6). The first EOF mode (Fig. 5a) accounts for 74.2% of the total variances and is characterized by the in-phase variation of meridional velocity with the largest amplitude situated at the mean velocity core position (as shown in Fig. 2a). According to the description[8, 34], this pattern corresponds to the transport mode, indicating the Kuroshio transport pulses superimposed on the mean structure along the 18°N section. It suggested that the first EOF mode denotes the mean spatial structure of the Kuroshio core along the 18°N section, while its time series represents the magnitude evolution of the Kuroshio transport. As shown in Fig. 5c, the normalized time series of the EOF1 reasonably well tracks the Kuroshio transport time series, with an unbelievable correlation coefficient of 0.99 above the 95% confidence level. Positive values of this mode indicate a pulse of increased meridional flow and larger transport and vice versa.

Relying on the lateral migration of the Kuroshio core appears as a dynamical model of anti-phase cancellation of the flow over the cross-section of meridional velocity[8,35]. In Fig. 6a, the second EOF mode is characterized by the anti-phase variation of meridional velocity with negative and positive values on the western-lower flank and the eastern-upper flank, respectively. The second EOF mode explains 11.6% of the total variances, where velocity increases on one side and velocity decreases on the other side, probably due to the migration of the Kuroshio core. Meantime, the anti-phase cancellation of the flow indicates less contribution to the Kuroshio transport along the overall section. Similarly, the time series of the EOF2 indicated the lateral migration of the Kuroshio core, where is the positive value corresponds to an offshore position for the Kuroshio core along the 18°N, vice versa (Fig. 6d). A composite analysis of the migration pattern (more than 1 standard deviation) is performed to obtain the in-shore phase (Fig. 6c) and the off-shore phase (Fig. 6e) of the Kuroshio core.

The first two modes of meridional velocity observed by mooring array at 18°N account for 85 % of the total variance in our measurements. Specifically, the result of EOF analysis using velocity observed exhibits a much stronger transport mode (74.2 %) than migration mode (11.6 %). This result has a difference from the Kuroshio east of Taiwan, Zhang et al.[8] found the transport and migration modes of the Kuroshio in the PCM1 array explain 34 % and 25 % of the total variances respectively, but Chang et al.[34] reported the first two dominant modes for the KTV1 array (the KTV1 array is located about 50 km south of the PCM-1 array) accounting for 29 % (transport mode) and 46 % (migration mode) of the total variance. It seems that the transport mode is dominant for the Kuroshio at 18°N, rather than the migration mode. We perform the same analysis on the meridional velocity simulated by HYCOM, which shows that the first two modes are migration modes (Fig. S3). But it is also found that the pattern in the mooring observation area (dotted frame) is consistent with the analysis result of the mooring array observation (Fig.5a and 6a). Focus on the amplitude of the meridional velocity in the first EOF mode simulated by HYCOM (Fig. S3a), the value near the shore is much smaller than that at the far shore (-20 cm/s vs 70 cm/s), so we believe that it is essentially a transport mode. This result has a great significance in understanding the structural variability of the Kuroshio east of Luzon.

Further research shows that the time series of the transport and migration modes of the Kuroshio at 18°N have a common 50–60 (~56) day periodic signal (Fig. 5b and 6b), which is consistent with the analysis results of the meridional velocity and the transport.

Discussion And Conclusion

Herein, utilizing the three mooring ADCPs direct measurements along 18°N section during January 2018 to February 2020 and HYCOM simulations data, the intraseasonal variation of the Kuroshio is investigated. The revelation that both the meridional velocity and volume transport at 18°N has an obvious ISV period of 50–60 days. Previous studies have found that westward propagating eddy-Kuroshio interaction processes account for the ISV of the Kuroshio at the Luzon Strait entrance[21], east of the Luzon Strait[32] and Taiwan[8,34]. Next, we will investigate whether the observed ISV of the Kuroshio at 18°N was associated with the mesoscale eddy activities.

To examine the validity of satellite data, Fig. S4 is the comparison between the mooring-observed meridional velocity averaged in 60–100 m and surface meridional geostrophic velocity from satellite altimeter at three mooring sites, which indicates that there is good consistency between them, and the all of correlation coefficients at the three station are greater than 0.8 with the 95% confidence level. Therefore, we can use the altimeter data to investigate the role of ocean eddies on the ISV of the Kuroshio. Review of previous research, the satellite altimetry demonstrates that there are very strong eddy activities near this region[25, 26, 36], such as Lien et al.[21] suggests cyclonic (anticyclonic) eddies decrease (increase) the zonal SLA slope and reduce (enhance) Kuroshio transport at the Luzon Strait entrance. In this study, the altimeter data also shows that the Kuroshio was affected by the eddies propagating westward. We have selected two cases for analysis, during the 12 August to 14 September 2018 and 23 May to 17 July 2019 (Fig. S4). Hereinafter referred to as the case 1 and the case 2. The basis for the selection is that the case 1 can be regarded as a process of intraseasonal phase of the Kuroshio from negative to positive (Fig. S4 and S2). On the contrary, the case 2 is a process of from a negative phase to a positive phase to next negative phase.

On 12 August 2018, the Kuroshio was controlled by an anticyclonic eddy (Fig. S5a) and then as a cyclonic eddy propagated westward (Fig. S5b–g), the ISV phase of the Kuroshio ushered in a negative phase on 30 August 2018 shown in Fig. S2b. Next, as the cyclone eddy moved northward and another anticyclone eddy propagated westward (Fig. S5g–l), the ISV phase of the Kuroshio gradually shifted to the next positive phase. The situation of case 2 is opposite to that of case1. Specifically, the Kuroshio was controlled by a cyclone eddy (Fig. S6a) –anticyclonic eddy (Fig. S6h) –cyclonic eddy (Fig. S6l) successively in case 2. This phenomenon illustrates that the phase of the Kuroshio experienced two transitions from negative phase to positive phase, and then from positive phase to next negative phase in case 2 shown in Fig. S2b and 10. Overall, the analysis of the two cases suggested that the Kuroshio will be controlled by the westward propagated of eddy from the Pacific Ocean.

Meantime, the surface intraseasonal meridional velocity observed by the altimeter propagates westward along an altitude of 18°N as clearly shown in Fig. 7a. The signal generated from the Pacific Ocean continues to propagate westward and reaches the coastal boundary. And the westward propagation speed was estimated to be 13.0 cm/s and the period is ~ 56 days. On the mooring observation area (Fig. 7b), which is basically consistent with the results observed by the mooring array (Fig. 7c). This further confirms that the ISV of the Kuroshio observed by the mooring array is caused by the regular imping of the eddies (with both the cyclonic and anticyclonic) that propagate westward from the Pacific.

A similar result is also demonstrated in the lag correlation maps of intraseasonal sea level anomaly (SLA) relative to its at 18°N, 123°E in Fig. 8. It shows the eddy-like patterns (with both cyclonic and anticyclonic polarities) generally propagated toward the west with the time lag increasing (reference marks A, B, and C), and continue to move northward after encountering the boundary (Fig. 8l). Based on the distance between A, B, and C, the wavelength was roughly estimated to be 6 degrees, which is about 633 km. This result is consistent with the result shown in Fig. 7a.

Nonetheless, issues remain. The westward propagation speed of eddies was estimated to be 13 cm/s, which is close to the phase speed (12.7 cm/s) of the first-mode baroclinic Rossby waves at the same latitude[37]. North of the mooring array area, Zheng et al.[38] analyze the interaction of nonlinear Rossby eddies with the Kuroshio used the satellite altimeter SLA data. Nonlinear Rossby eddy trains, consisting of the cyclonic and anticyclonic mesoscale eddies and originating from the tropical Pacific, propagate westward. This phenomenon is very similar to the results shown in this article (Fig. S5, S6, and 14). Therefore, we guess that the Kuroshio at 18°N may also be affected by the nonlinear Rossby eddy trains. This needs to be discussed further in future work.

In addition, there is an eddy abundant region east of the mooring array, the eddy generated through the baroclinic instability of the surface eastward flowing STCC and the subsurface westward flowing NEC system[25–29]. The above analysis shows that the eddies that dominate the ISV of the Kuroshio mainly come from the open ocean. So, we suggest that the westward propagating eddies may be generated from the instability of the vertically sheared STCC-NEC system.

Methods

To monitor the spatial structure and temporal variability of the meridian current east of Luzon Island, three moorings (labeled M1, M2, and M3) were deployed along ~ 18°N latitude (122.7°E, 123°E, and 123.3°E). The distance between each mooring roughly 32 km, and M1 is about 54 km away from the coast (Fig. 1a). The location of M1 is basically the same as the location of mooring in Hu et al.[22](18.02°N, 122.63°E) and Chen et al. [24] (17.96°N, 122.93E). As shown in Fig. 1b, 1c, and 1d, the observation period of all moorings started on January 25, 2018, and the time span is 838 days, 766 days, 791 days, respectively. Each mooring was equipped with one upward-looking and one downward-looking 75 kHz Teledyne RD Instruments (TRDI) ADCP at ~ 400 m depth to measure the current velocity ranges from the sea surface to about 900 m. The ADCP measured velocity every 1 hour in 60 bins with a bin size

of 8 m. In this study, only the upward-looking ADCP data are used to investigate the current as shown in Fig. 1b, 1c, and 1d, since the data of the M2's downward measurement was missing and our objective is to explore the ISV characteristics of the upper layer Kuroshio. Firstly, the observed raw data was daily averaged to remove the tidal signal and then the velocity data were interpolated to a uniform 10 m intervals in vertical. About the quality control, only the data with a percent good beam larger than 80% is considered. Most of ADCP data in the surface layer (upper 50 m) cannot pass through quality control owing to the echo of beam emission is very strong, thence, the obtained surface data unavailable is deleted for simplicity. Finally, the daily meridional velocity data was smoothed for 7-day. This process can exclude the high frequency signals such as tides and internal waves. According to the span time as shown in Fig. 1b, 1c, and 1d, we choose the time shared by the three moorings to carry out the following research, totaling 766 days, from January 25, 2018, to February 29, 2020.

Data sources

The mooring ADCP data used during the current study are available from the corresponding author on reasonable request. The 1/4-degree gridded sea level anomalies (SLA) and absolute geostrophic meridional and zonal velocity in delayed-time allsat series was obtained from Copernicus Marine Environment Monitoring Service (http://marine.copernicus.eu/). And the daily meridional velocity data from the global Hybrid Coordinate Ocean Model (HYCOM) 1/12-degree GOFS 3.1 analysis output on the GLBv0.08 grid. which are downloaded from https://www.hycom.org/dataserver/gofs-3pt1/analysis.

Declarations

Acknowledgments

We are sincerely grateful to all the investigators and the crew of R/V Kexue (Science) for their effort in deployments and recoveries of moorings. This study is supported by the National Natural Science Foundation of China (grants 41976011, 91858101), and the National Key Research and Development Program of China (grant 2017YFA0604102).

Author Contributions

X.Y. analyzed the data and wrote the manuscript. Q.W. and D.H. supervised the work and contributed to the polish of the manuscript. J.M. and S.H. participated in discussions on the topic of research. All authors reviewed and approved the final version of the manuscript.

References

1. Nitani, H. Beginning of the Kuroshio. In: Stommel, H., Yoshida, K. Kuroshio: Its Physical Aspects. 129–163 (Univ. of Wash. Press, 1972).
2. Ma, X. et al. Western boundary currents regulated by interaction between ocean eddies and the atmosphere. *Nature* **535**, 533–537 (2016).

3. Centurioni, L.R., Niiler, P.P. & Lee, D.K. Observations of inflow of Philippine Sea surface water into the South China Sea through the Luzon Strait. Journal of Physical Oceanography 34, 113–121 (2004).
4. Liang, W.D., Yang, Y.J., Tang, T.Y. & Chuang, W.S. Kuroshio in the Luzon Strait. *J. Geophys. Res.-Oceans* **113**, C08048 (2008).
5. Andres, M. et al. Downstream evolution of the Kuroshio's time-varying transport and velocity structure. *J. Geophys. Res.-Oceans* **122**, 3519–3542 (2017).
6. Mensah, V., Jan, S., Chiou, M.D., Kuo, T.H. & Lien, R.C. Evolution of the Kuroshio Tropical Water from the Luzon Strait to the east of Taiwan. *Deep-Sea Research Part I-Oceanographic Research Papers* **86**, 68–81 (2014).
7. Yang, Y., Liu, C.-T., Hu, J.-H. & Koga, M. Taiwan Current (Kuroshio) and Impinging Eddies. *Journal of Oceanography* **55**, 609–617 (1999).
8. Zhang, D.X., Lee, T.N., Johns, W.E., Liu, C.T. & Zantopp, R. The Kuroshio east of Taiwan: Modes of variability and relationship to interior ocean mesoscale eddies. *Journal of Physical Oceanography* **31**, 1054–1074 (2001).
9. Johns, W.E. et al. The Kuroshio east of Taiwan: Moored transport observations from the WOCE PCM-1 array. *Journal of Physical Oceanography* **31**, 1031–1053 (2001).
10. Lee, I.H., Ko, D.S., Wang, Y.-H., Centurioni, L. & Wang, D.-P. The mesoscale eddies and Kuroshio transport in the western North Pacific east of Taiwan from 8-year (2003–2010) model reanalysis. *Ocean Dynamics* **63**, 1027–1040 (2013).
11. Jan, S. et al. Large variability of the Kuroshio at 23.75°N east of Taiwan. *Journal of Geophysical Research: Oceans* **120**, 1825–1840 (2015).
12. Yang, D.Z. et al. Numerical study on the pattern and origins of Kuroshio branches in the bottom water of southern East China Sea in summer. *J. Geophys. Res.-Oceans* **117**, C02014 (2012).
13. Wang, J. & Oey, L.Y. Seasonal Exchanges of the Kuroshio and Shelf Waters and Their Impacts on the Shelf Currents of the East China Sea. *Journal of Physical Oceanography* **46**, 1615–1632 (2016).
14. Andres, M. et al. Observations of Kuroshio flow variations in the East China Sea. *J. Geophys. Res.-Oceans* **113**, C05013 (2008).
15. Wang, Q., Tang, Y.M., Pierini, S. & Mu, M. Effects of Singular-Vector-Type Initial Errors on the Short-Range Prediction of Kuroshio Extension Transition Processes. *Journal of Climate* **30**, 5961–5983 (2017).
16. Imawaki, S. et al. Satellite altimeter monitoring the Kuroshio transport south of Japan. *Geophysical Research Letters* **28**, 17–20 (2001).
17. Qiu, B. & Chen, S.M. Variability of the Kuroshio Extension jet, recirculation gyre, and mesoscale eddies on decadal time scales. *Journal of Physical Oceanography* **35**, 2090–2103 (2005).
18. Kakinoki, K. et al. Variations of Kuroshio geostrophic transport south of Japan estimated from long-term IES observations. *Journal of Oceanography* **64**, 373–384 (2008).

19. Rudnick, D.L., Jan, S. & Lee, C.M. A New Look at Circulation in the Western North Pacific INTRODUCTION TO THE SPECIAL ISSUE. *Oceanography* **28**, 16–23 (2015).
20. Gordon, A.L., Flament, P., Villanoy, C. & Centurioni, L. The nascent Kuroshio of Lamon Bay. *J. Geophys. Res.-Oceans* **119**, 4251–4263 (2014).
21. Lien, R.C. et al. Modulation of Kuroshio transport by mesoscale eddies at the Luzon Strait entrance. *J. Geophys. Res.-Oceans* **119**, 2129–2142 (2014).
22. Hu, D.X. et al. Direct Measurements of the Luzon Undercurrent. *Journal of Physical Oceanography* **43**, 1417–1425 (2013).
23. Wang, Q.Y., Zhai, F.G. & Hu, D.X. Variations of Luzon Undercurrent from observations and numerical model simulations. *J. Geophys. Res.-Oceans* **119**, 3792–3805 (2014).
24. Chen, Z.H. et al. Strengthening Kuroshio observed at its origin during November 2010 to October 2012. *J. Geophys. Res.-Oceans* **120**, 2460–2470 (2015).
25. Qiu, B. Seasonal eddy field modulation of the North Pacific subtropical countercurrent: TOPEX/Poseidon observations and theory. *Journal of Physical Oceanography* **29**, 2471–2486 (1999).
26. Yang, G., Wang, F., Li, Y.L. & Lin, P.F. Mesoscale eddies in the northwestern subtropical Pacific Ocean: Statistical characteristics and three-dimensional structures. *J. Geophys. Res.-Oceans* **118**, 1906–1925 (2013).
27. Hwang, C., Wu, C.R. & Kao, R. TOPEX/Poseidon observations of mesoscale eddies over the Subtropical Countercurrent: Kinematic characteristics of an anticyclonic eddy and a cyclonic eddy. *J. Geophys. Res.-Oceans* **109**, C08013 (2004).
28. Qiu, B. & Chen, S.M. Interannual Variability of the North Pacific Subtropical Countercurrent and Its Associated Mesoscale Eddy Field. *Journal of Physical Oceanography* **40**, 213–225 (2010).
29. Roemmich, D. & Gilson, J. Eddy Transport of Heat and Thermocline Waters in the North Pacific: A Key to Interannual/Decadal Climate Variability? *J.phys.oceanogr* **13**, 675–688 (2001).
30. Tsai, C.J. et al. Eddy-Kuroshio interaction processes revealed by mooring observations off Taiwan and Luzon. *Geophysical Research Letters* **42**, 8098–8105 (2015).
31. Rudnick, D.L. et al. Seasonal and Mesoscale Variability of the Kuroshio Near Its Origin. *Oceanography* **24**, 52–63 (2011).
32. Zhang, Z.W., Zhao, W., Tian, J.W., Yang, Q.X. & Qu, T.D. Spatial structure and temporal variability of the zonal flow in the Luzon Strait. *J. Geophys. Res.-Oceans* **120**, 759–776 (2015).
33. Liang, W.D., Tang, T.Y., Yang, Y.J., Ko, M.T. & Chuang, W.S. Upper-ocean currents around Taiwan. *Deep-Sea Research Part Ii-Topical Studies in Oceanography* **50**, 1085–1105 (2003).
34. Chang, M.H. et al. Zonal migration and transport variations of the Kuroshio east of Taiwan induced by eddy impingements. *Deep-Sea Research Part I-Oceanographic Research Papers* **131**, 1–15 (2018).
35. Johns, W.E. & Schott, F. Meandering and Transport Variations of the Florida Current. *Journal of Physical Oceanography* **17**, 1128–1147 (1987).

36. Liu, Y. et al. Eddy analysis in the subtropical zonal band of the North Pacific Ocean. *Deep-Sea Research Part I-Oceanographic Research Papers* **68**, 54–67 (2012).
37. Chelton, D.B., DeSzoeke, R.A., Schlax, M.G., El Naggar, K. & Siwertz, N. Geographical variability of the first baroclinic Rossby radius of deformation. *Journal of Physical Oceanography* **28**, 433–460 (1998).
38. Zheng, Q. et al. Satellite altimeter observations of nonlinear Rossby eddy–Kuroshio interaction at the Luzon Strait. *Journal of Oceanography* **67**, 365–376 (2011).

Figures

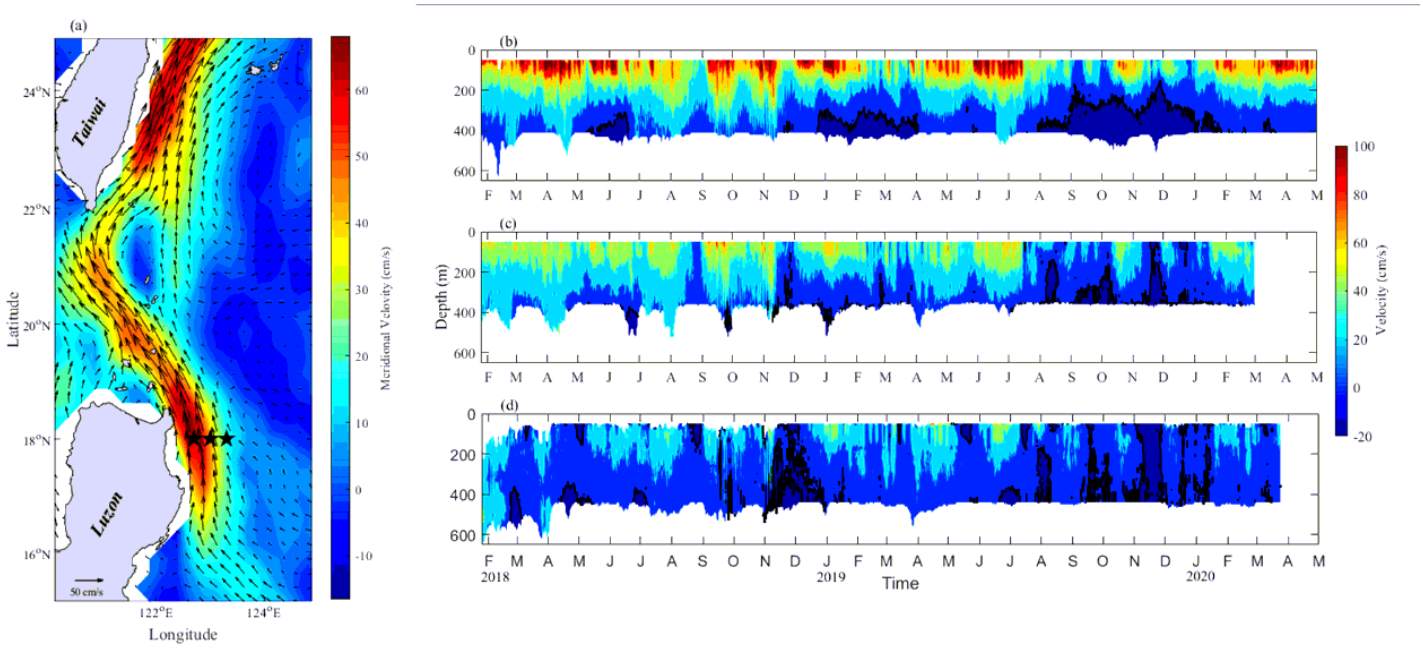

Figure 1

(a) The mean meridional velocity (colour, cm/s) and the mean geostrophic current (vector, cm/s) at surface from the satellite altimetry within the time span of the mooring observation. The three stars indicate the locations of the three moorings east of Luzon. The observed daily meridional velocity (cm/s) at (b) 122.7°E (M1), (c) 123°E (M2), and (d) 123.3°E (M3) along 18°N. The black line represents the zero contour in (b), (c), and (d). Figures are plotted using MATLAB R2019a (http://www.mathworks.com/). Note: The designations employed and the presentation of the material on this map do not imply the expression of any opinion whatsoever on the part of Research Square concerning the legal status of any country, territory, city or area or of its authorities, or concerning the delimitation of its frontiers or boundaries. This map has been provided by the authors.

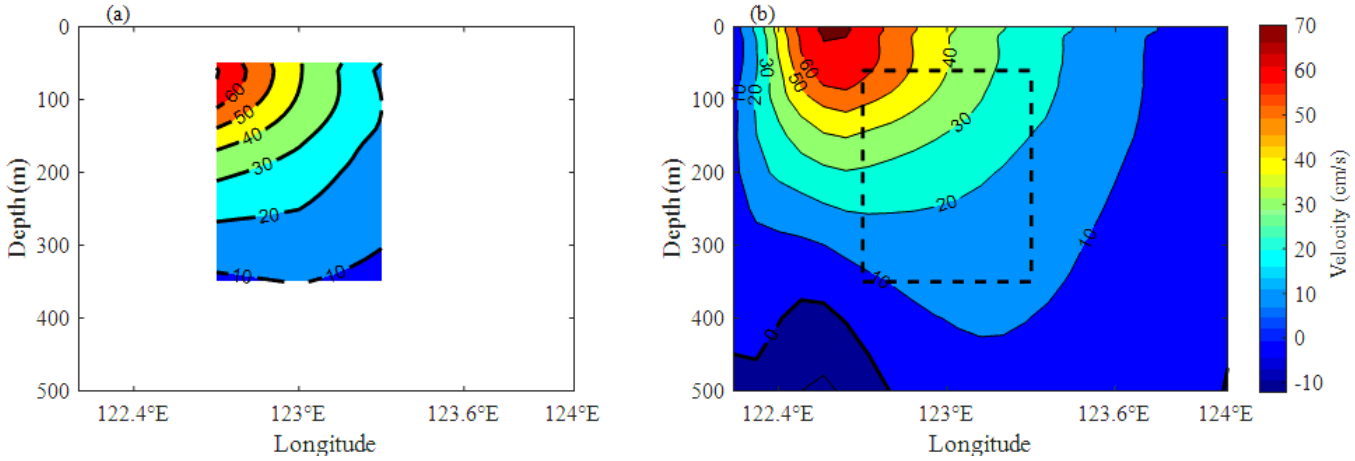

Figure 2

(a) The mean meridional velocity along the 18 °N section of mooring observation. (b) same as (a) but from HYCOM simulation during the mooring observation period. The observation range (122.7°E–123.3°E, 60–350 m) of the moored ADCPs array shown in (a) is also indicated in (b, dotted box). Figures are plotted using MATLAB R2019a (http://www.mathworks.com/).

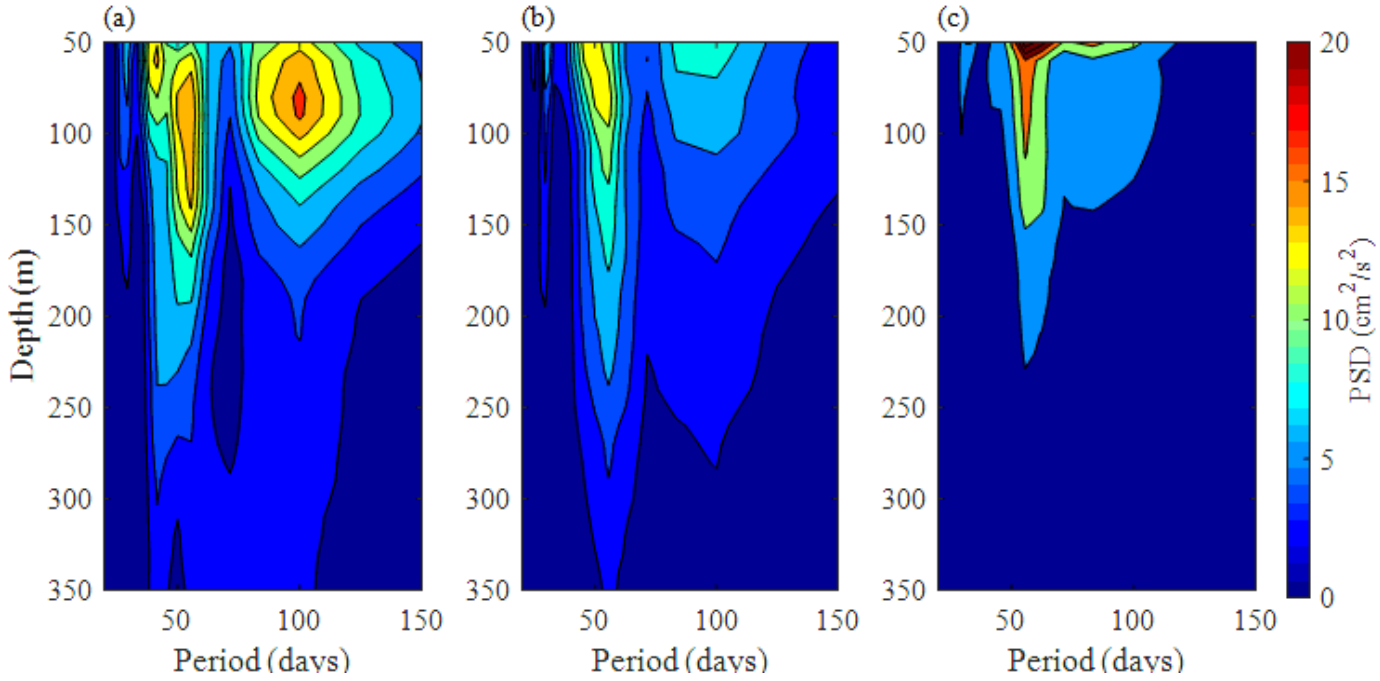

Figure 3

Power spectrum density (PSD) of the 20–120 days filtered meridional velocity at M1 (a), M2 (b), and M3 (c). Figures are plotted using MATLAB R2019a (http://www.mathworks.com/).

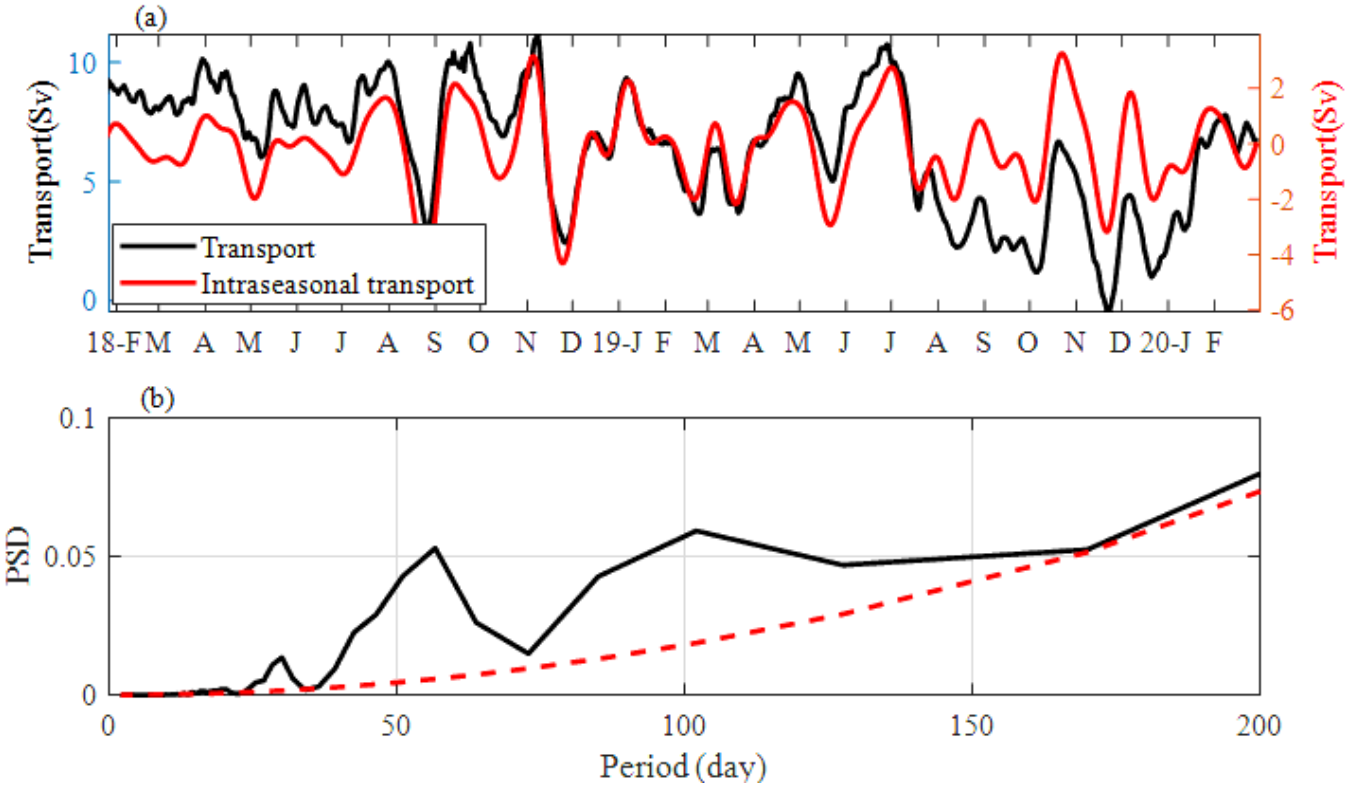

Figure 4

(a) Time series of the Kuroshio transport (black line) and the transport in the 20–120-day band (red line). (b) Power spectrum density of the transport. The red dashed line in (b) denotes the 95% confidence level. Figures are plotted using MATLAB R2019a (http://www.mathworks.com/).

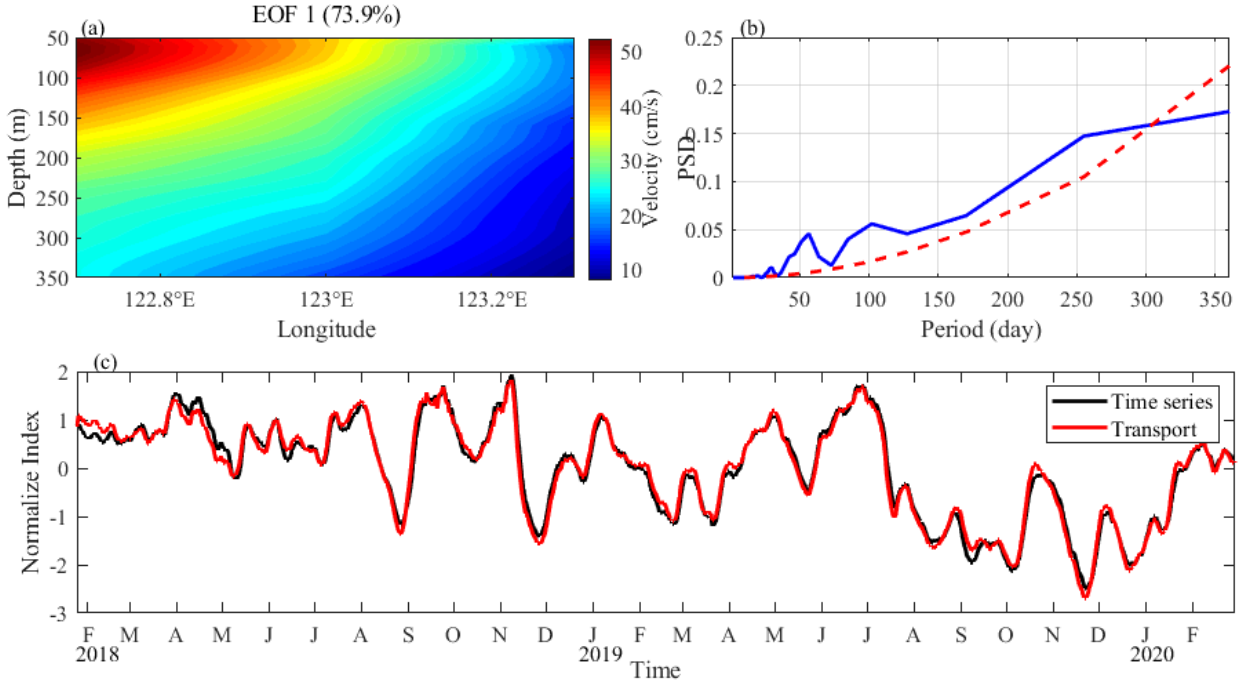

Figure 5

(a) The first EOF mode of meridional velocity observed by mooring array at 18°N. (b) The PSD of the time series of the EOF1. (c) Comparison between the normalized time series of the observed Kuroshio transport (red line) and the time series of the EOF1(black line). The red dashed line in (b) denotes the 95% confidence level. Figures are plotted using MATLAB R2019a (http://www.mathworks.com/).

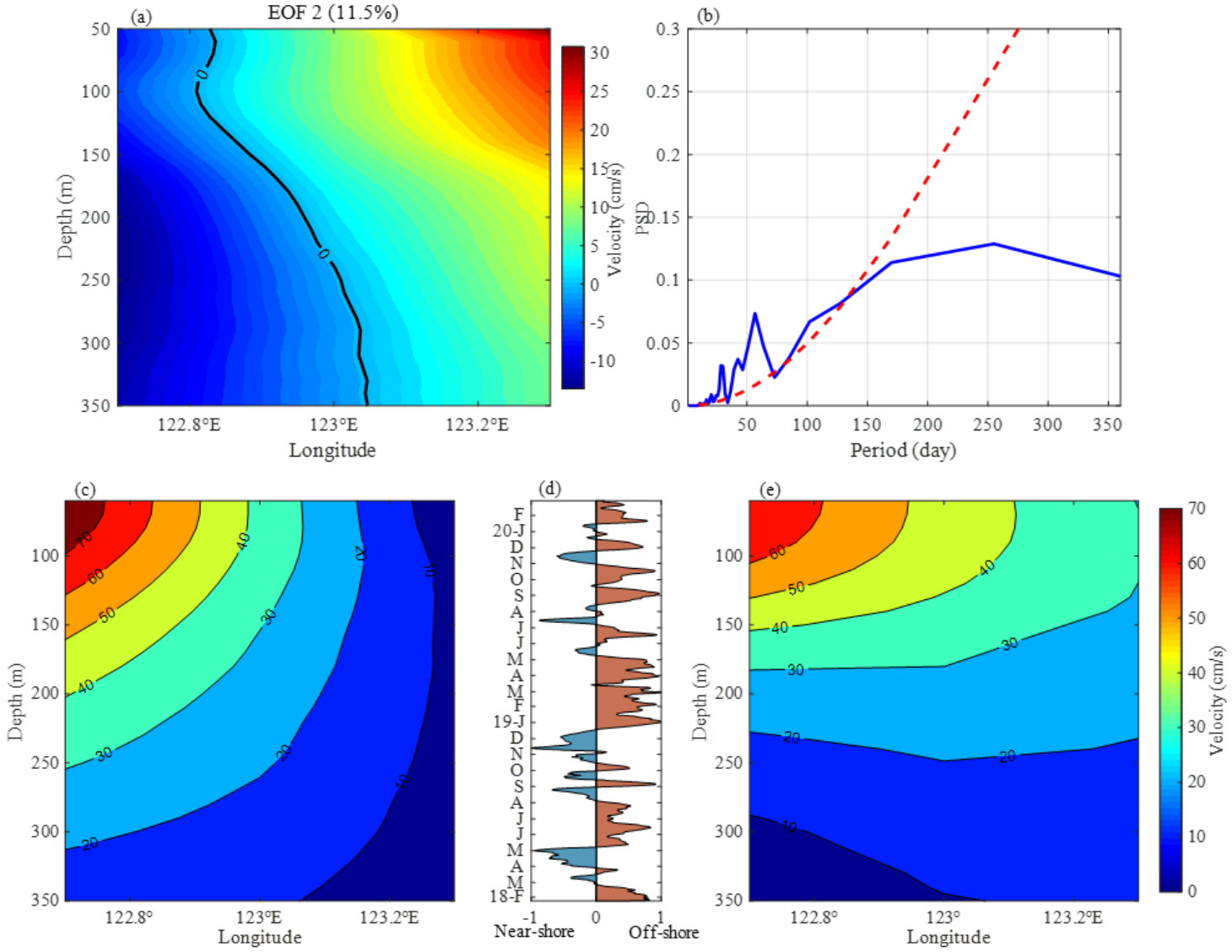

Figure 6

(a) The second EOF mode of meridional velocity from mooring observations. (d) The normalize time series of the second EOF mode. (b) The PSD of the time series of the second EOF mode shown in (d). The composited meridional velocity (cm/s) of the Kuroshio when the time series of the EOF2 is greater than 1 standard deviation (c) and less than -1 standard deviation(e). The red dashed line in (b) denote the 95% confidence level. The bipolar directions of the X-axis in (d) represent the near-shore (-1) and off-shore (+1) position of the Kuroshio core. Figures are plotted using MATLAB R2019a (http://www.mathworks.com/).

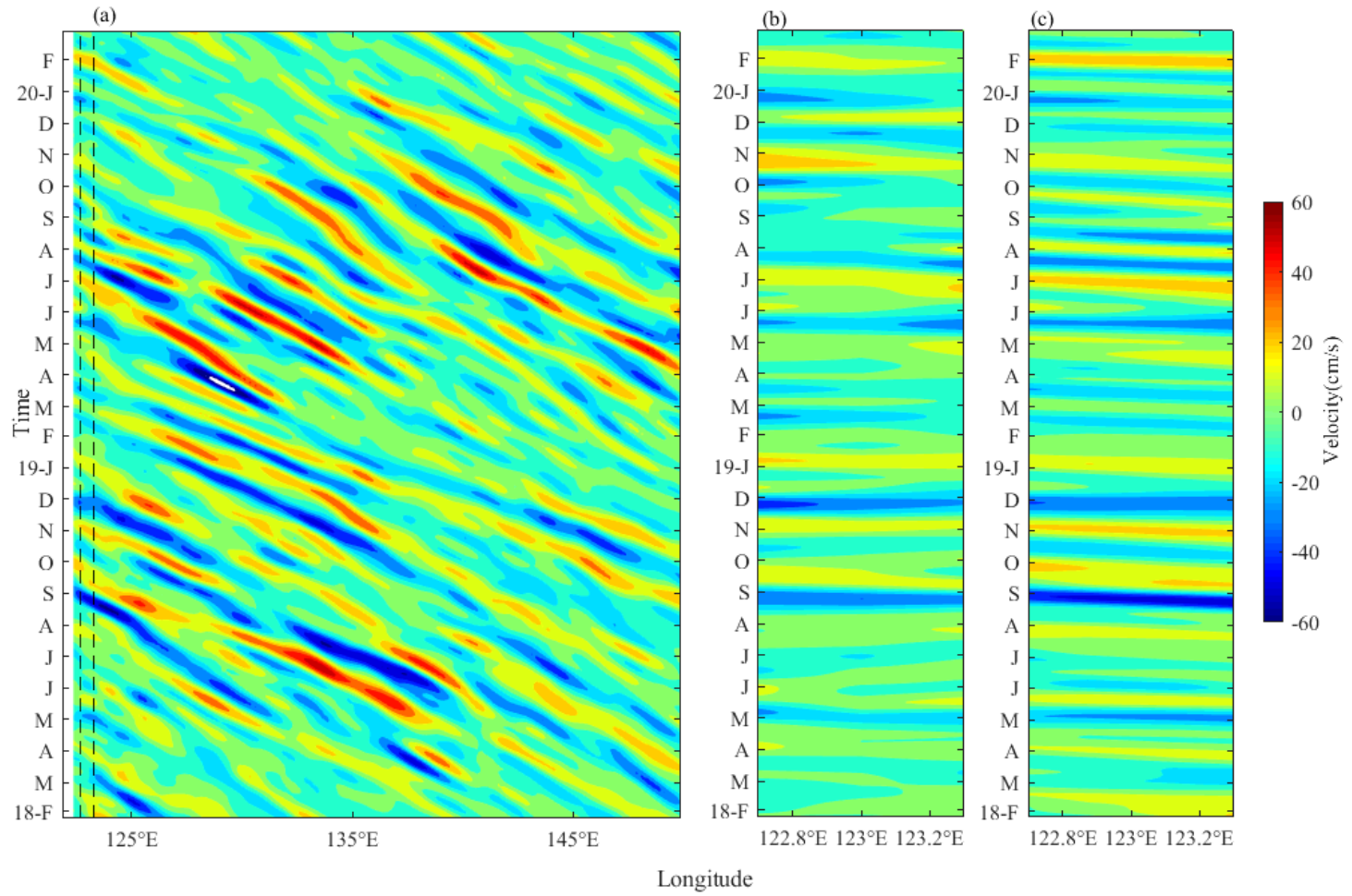

Figure 7

(a) Longitude-time plot of the surface meridional geostrophic velocity in 20-120-day filter from altimeter along the 18°N. (b) Same as (a) but between 122.7°E and 123.3°E indicated by two dashed line in (a). (c) Longitude-time plot of the observed 20-120-day meridional velocity vertically averaged in 60-100 m depth. Figures are plotted using MATLAB R2019a (http://www.mathworks.com/).

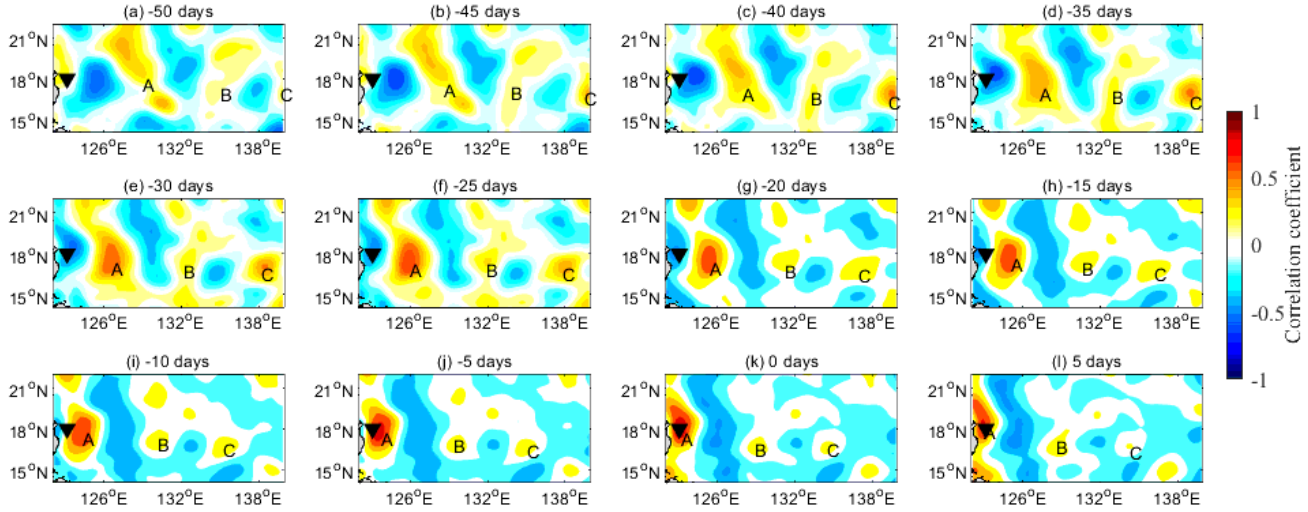

Figure 8

The correlation coefficient between intraseasonal SLA and the intraseasonal SLA at a fixed point (18°N, 123.125°E) when the former lag the latter for from -50 days (a) to 5 days (l) every five days. The black triangle (18°N, 123°E) denotes the position of the mooring. The A, B, and C are the marks for the eddies. Figures are plotted using MATLAB R2019a (http://www.mathworks.com/).

Supplementary Files

This is a list of supplementary files associated with this preprint. Click to download.

- SupplementaryInformation.pdf